CCS Chemistry

RESEARCH ARTICLE

Received: Apr. 16, 2021 | Accepted: July 16, 2021

Hierarchical Microphase Behaviors of Chiral Block Copolymers under Kinetic and Thermodynamic Control

Zhen Geng[1], Huiying Wang[1], Seon-Mi Jin[2], Xinghao Yan[3], Min Ren[1], Bijin Xiong[1], Ke Wang[1], Renhua Deng[1], Senbin Chen[1], Eunji Lee[2], Lianbin Zhang[1]*, Jintao Zhu[1]* & Zhenzhong Yang[3]

[1]*State Key Laboratory of Materials Processing and Die & Mould Technology, Key Laboratory of Materials Chemistry for Energy Conversion and Storage of Ministry of Education, School of Chemistry and Chemical Engineering, Huazhong University of Science and Technology, Wuhan 430074,* [2]*School of Materials Science and Engineering, Gwangju Institute of Science and Technology (GIST), Gwangju 61005,* [3]*Institute of Polymer Science and Engineering, Department of Chemical Engineering, Tsinghua University, Beijing 100084*

**Corresponding authors: jtzhu@mail.hust.edu.cn; zhanglianbin@hust.edu.cn*

Cite this: *CCS Chem.* **2021**, *3*, 2561–2569

Chiral superstructures in confined spaces are subtly affected by the complex interplay among various noncovalent interactions, details of which are still in adequately understood. Herein, we report the three-dimensional confined assembly of the chiral block copolymers of polystyrene-*block*-poly(D-lactide) and its enantiomer in emulsion droplets and demonstrate unprecedented successive microphase transformations from single helices to double helices with inverted helicity, and then to twisted cylinders in the constructed colloidal particles. The above hierarchical structural transformations of chiral microphases are kinetically dependent and can further transform into thermodynamically stable achiral cylinders with saddle-shaped topology upon solvent annealing. The formation and subsequent structural transformations as well as the final degeneration of chiral architectures provide guidance to understand the chiral evolution at different length scales within spherical confined space and to fabricate biomimetic systems.

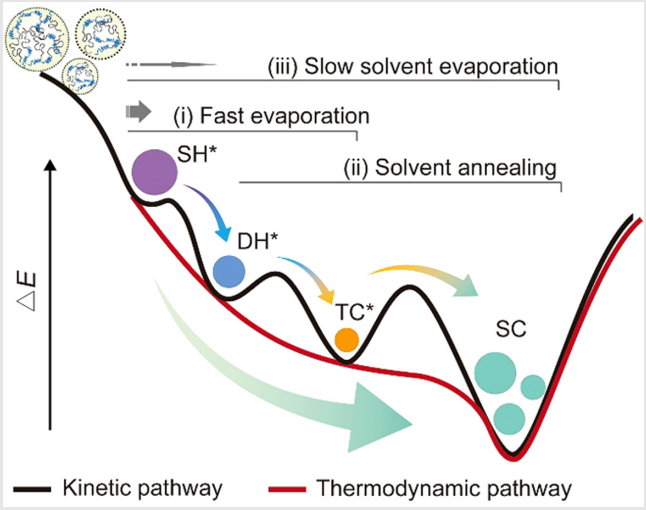

Keywords: **chiral block copolymers, helical structures, confined assembly, kinetic control, mesoporous chiral nanochannels**

Introduction

Chirality can be universally observed at various hierarchical levels from microscopic (i.e., in helical neutrinos, most amino acids, and double-helical DNA) to macroscopic and galactic scales.[1,2] Deeply understanding the origination of chirality and thereby constructing chiral entities is intensely appealing in chemistry and materials science due to the intriguing optical and electronic properties arisen from the chiral features.[3–5] Generally, bottom-up self-assembly of elaborately designed molecules or building blocks with chiral features has been

DOI: 10.31635/ccschem.021.202101067
CCS Chem. **2021**, *3*, 2561–2569

proven as an efficient route to fabricate chiral entities with hierarchical architectures at different length scales.[6–8] Block copolymers (BCPs) composed of helical segments (denoted as chiral block copolymers, BCPs*) are one of the ideal candidates for the bottom-up self-assembly, bringing various complicated chiral superstructures.[9–12] Insights into the mechanism indicate that the formation of chiral surperstructures are kinetically dependent and affected by the complex interplay among multiple interactions including chirality, hydrophibicity, and crystallization, the details of which, however, are still inadequately understood.[13–15]

Physiological processes and biological reactions are carried out well in nanoconfinement space where the spatial confinement plays a significant role in the sophisticated biochemical reactions.[16–18] For example, spatial DNA confinement *in vivo* promotes the formation of localized defects at mechanically weak sites which are vital for biological regulatory functions.[17] Inspired by nature, self-assembly of BCPs in confined spaces is utilized to generate intriguing hierarchical superstructures which are generally unavailable either in bulk or in solution.[19–21] Especially, colloidal particles containing helical internal microphases can be constructed under three-dimensional (3D) confined conditions.[22,23] Nevertheless, the chirality of those helical microphases is always random, and their architectures cannot be well controlled. It is anticipated that if BCPs* self-assemble in 3D confined geometries, the chiral transfer of helical block from conformation to microphase would afford opportunities to fabricate sophisticated chiral architectures with controllable helicity. However, to the best of our knowledge, there are so far no relevant attempts to disclose the effect of 3D confinement on the chiral transfer of BCPs*. Therefore, investigations on the fabrication of chiral architectures from the 3D confined assembly of BCPs* and in-depth understanding of their formation dynamics in the confined space are essential and extremely desirable.

Herein, we report unprecedented hierarchical microphase behaviors based on the 3D confined assembly of BCPs* of polystyrene-*block*-poly(D-lactide) (PS-*b*-PDLA) triggered by organic solvent evaporation in emulsion droplets, where the spherical interface of the emulsion droplet acts as the 3D confined boundary (see Experimental Details in Supporting Information). When the organic solvent evaporates rapidly, successive structural transformations of PDLA microphases occur during the formation of colloidal particles (Figure 1, i) from single helices (SH*) to double helices (DH*) and then to twisted cylinders (TC*). Solvent annealing induces the above chiral microphases to transform them to thermodynamic achiral saddle-shaped cylinders (SC) (Figure 1, ii). Alternatively, colloidal particles containing the same SC can be constructed when the organic solvent is allowed to evaporate slowly (Figure 1, iii).

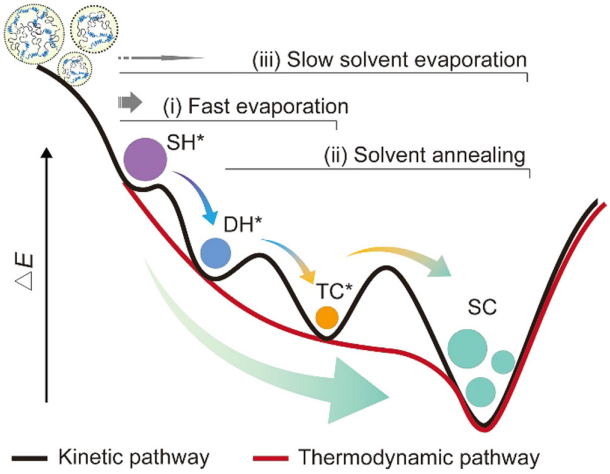

Figure 1 | *Schematic illustration of the hierarchical structural transformations of chiral microphases in colloidal particles during the 3D confined assembly of BCPs* under kinetic and thermodynamic control. Solid spheres with different colors represent colloidal particles containing different kinds of microphases.*

Experimental Methods

Preparation of the colloidal particles containing chiral microphases

We used the emulsion-solvent evaporation method to prepare the colloidal particles. Typically, PS-*b*-PDLA was dissolved in chloroform at an initial concentration ($C_{initial}$) of 10 mg/mL. Afterward, 0.1 mL of the polymer solution was emulsified with 1.0 mL aqueous solution of sodium dodecyl sulfate (SDS) via membrane-extrusion emulsification.[1] The resulting emulsions were poured into a 50 mL beaker and diluted by adding another 0.5 mL of the same surfactant aqueous solution. Chloroform was then allowed to evaporate quickly by gently shaking the beaker at room temperature. After nearly 1 min, the milky emulsions turned into a transparent state, implying the formation of polymer particles.

Solvent annealing

In the solvent annealing process, 0.25 mL of the colloidal particle suspension was first diluted by 0.25 mL SDS suspension (3 mg/mL). Afterward, the diluted suspension with particle content of ~0.17 mg/mL in a small vial (5 mL) was placed inside a large vial (25 mL) with 1.0 mL of $CHCl_3$ and kept for 2 days at 30°C. Afterward, the inner small vial was taken out and placed into the ambient atmosphere for 12 h at room temperature to release the absorbed $CHCl_3$ before further characterization.

DOI: 10.31635/ccschem.021.202101067
CCS Chem. **2021**, *3*, 2561–2569

Preparation of colloidal particles under slow solvent evaporation condition

In the control experiment in which the slow evaporation method was used, the emulsions prepared from membrane-extrusion of 0.1 mL of the polymer solution and 1.0 mL aqueous solution of SDS were mixed with another 0.5 mL of SDS suspension (3 mg/mL) and then poured into a 10 mL vial with a height of ~4.5 cm and an inner diameter of ~2 cm. The open vial was then placed under room temperature for 2 days before characterization.

Results and Discussion

Colloidal particles containing chiral microphases prepared under rapid solvent evaporation condition

The solvent evaporation rate has been reported as a critical parameter in determining the microphase nanostructre and final shape of the colloidal particles prepared from 3D confined assembly of BCPs.[24–26] By changing this parameter, the self-assemby kinetics of BCPs could be efficiently tuned.[25] Meanwhile, rapid solvent evaporation has been proven as a prerequisite for the formation of the chiral microphase from the bulk self-assembly of BCPs*.[27,28] Therefore, 3D confined assembly of PS-*b*-PDLA under the rapid solvent evaporation condition was initially studied. Colloidal particles containing regularly coiled cylindrical PDLA microphases were shown in the transmission electron microscopy (TEM) images after selectively staining the PS microphase by ruthenium tetroxide (RuO_4) (Figure 2a). To get a clearer picture of the nanostructures in the colloidal particles, PDLA microdomains were hydrolyzed before TEM observation to enhance the contrast of PDLA and PS microphases (Supporting Information Figure S1). PDLA cylinders exhibited fascinating chiral topologies including *P*-helical SH* (Figure 2b and Supporting Information Figure S2), DH* (Figure 2c), TC* (Figure 2d), and mixtures of DH* and TC* (Figure 2e). The 3D tomography TEM technique was utilized to more clearly recognize the helicity of DH* and TC* (Supporting Information Figures S3 and S4 and Videos S1 and S2). The reconstructed TEM results showed that both the DH* and TC* topologies possessed *M*-helicity. Moreover, the topologies of chiral PDLA cylinders (i.e., SH*, DH*, and TC*) were found to be curvature-dependent (Figure 2f). PDLA microphases with the above three chiral topologies coexisted in colloidal particles with large sizes (D, $D > 200$ nm). Smaller particles (150 nm < D < 200 nm) contained a mixture of TC* and DH* structures while TC* was dominant within particles smaller than 150 nm. Therefore, the chiral topology of PDLA microphase in colloidal particles could be readily controlled by tuning the particle size. For instance, increasing the initial BCPs* concentration ($C_{initial}$) afforded larger particles and thus raised the fraction of colloidal particles containing the PDLA microphase with DH* and TC* topologies, whereas decreasing the $C_{initial}$ resulted in particles containing more TC* microphases (Figure 2f and Supporting Information Figures S5–S7). The chemical composition for the surface of colloidal particles was revealed to consist of both PDLA and PS microphases, indicating a roughly neutral interfacial affinity for the two blocks (Figure 2g and Supporting Information Table S1). Furthermore, the one-dimensional small-angle X-ray scattering (1D SAXS) profile was utilized to investigate the microphase structure within the colloidal particles. The reflections at the relative q^* values of $1{:}\sqrt{3}{:}\sqrt{4}{:}\sqrt{7}$ could be found, suggesting a hexagonally packed cylindrical structure (Figure 2h). The lattice parameter (a = 29.5 nm) was very consistent with the observed value in TEM tomography results (Supporting Information Figure S3).

Hierarchical microphase transformations under kinetic control

We propose that the formation of the above three chiral topologies of PDLA microphase is involved in chiral transfer and successive microphase transformations during the confined assembly of PS-*b*-PDLA (Figure 3a). Homochiral transfer from chain conformation to microphase is responsible for the formation of PDLA cylindrical microphase with SH* topology, which is similar to the formation of helical cylinders from bulk self-assembly of PS-*b*-PDLA.[27,28] The circular dichroism (CD) spectra of PS-*b*-PDLA in $CHCl_3$ and within the colloidal particles indicate the helical conformation of the PDLA blocks (Figure 3b and Supporting Information Figure S8). Interchain packing of PDLA leads to specific helical steric hindrance and results in twisting and shifting of PDLA microdomains into SH* topology (Supporting Information Figure S9). In this process, the PS blocks are forced to stretch along with the twisted PS/PDLA interface, causing entropy loss of PS chains and giving rise to internal stress within the PS microphase around PDLA cylinders (Figure 3a, i). Subsequently, the preformed SH* spontaneously transformed into DH* to eliminate the accumulated internal stress (Figure 3a, ii). The gradual shrinking of the spherical confined boundary is beneficial for this entropy-driven microphase transformation. We used two adjacent rubber bands as a model to get a better understanding of the above transformation process which is illustrated in Figure 3d. Colloidal particles containing exclusive SH* are minor even in ones that are micrometre-sized (Supporting Information Figure S10), further verifying that the DH* microphases possessed lower free energy than SH* structures. The coexistence of DH* and TC* topologies along with one individual PDLA cylinder are commonly found (Figure 2e and Supporting Information Video S1), suggesting that TC* results from DH* through the collapse and

DOI: 10.31635/ccschem.021.202101067
CCS Chem. **2021**, *3*, 2561–2569

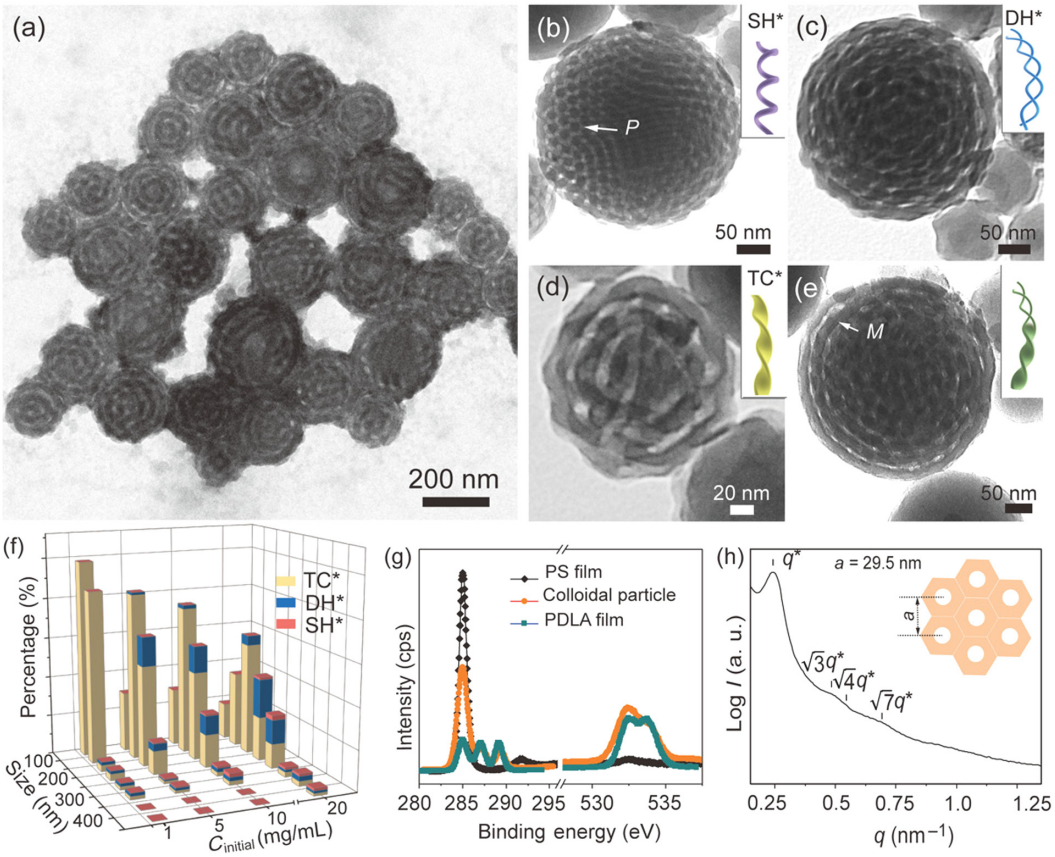

Figure 2 | *Characterization of PS-b-PDLA colloidal particles. (a) TEM images of the colloidal particles. Samples were stained with RuO_4 before TEM characterization. (b–e) Representative magnified TEM images of colloidal particles containing PDLA microphase mainly exhibiting chiral architectures of P-helical SH*, DH*, TC*, and coexisting TC* and DH* structures along with one single cylinder, respectively. (f) Size statistics of the colloidal particles prepared from different $C_{initial}$ conditions categorized by the topologies of PDLA cylinders within the particles (i.e., SH*, DH*, and TC*). Statistical results were calculated from TEM images of colloidal particles etched by formic acid before characterization. (g) XPS C 1s and O 1s spectra of PS and PDLA films and colloidal particles of PS-b-PDLA. (h) SAXS profile of PS-b-PDLA colloidal particles. The cartoon image illustrates the periodic space length (a, which is calculated from q*, q* = 0.2459) and the hexagonal packed PDLA cylindrical microphase within the PS matrix.*

fusion of the two screwed cylinders of DH*. During the transformation from DH* to TC*, the helicity of DH* is accordingly transferred, which explains that the handedness of TC* is identical with DH* but the opposite of the helicity of SH*. Fusion of the two screwed cylinders of DH* into TC* decreases the PDLA/PS interface area and thus minimizes the interfacial energy (Figure 3a, iii), indicating that this microphase transformation is enthalpy-driven.[29,30] Moreover, TC* topology is dominated in relatively small colloidal particles, implying that the structural transformation from DH* to TC* is also promoted by the confinement effect. In summary, chiral transfer-induced SH* formation and hierarchical microphases transformations—from SH* to DH* and then to TC*—take place during the confined assembly of PS-*b*-PDLA in an emulsion droplet. The statistical average section-diameters (<*d*>) of PDLA microphases along with curvature (*K*) in the colloidal particles are very consistent with the above proposed hierarchical microphase transformations (Figure 3c) (see detailed discussion in Supporting Information Figure S11). The confined assembly of BCPs* of PS-*b*-PLLA was also investigated, and similar results were found, comparing them with PS-*b*-PDLA (Supporting Information Figures S12 and S13). As expected, PLLA microphases exhibiting SH*, DH*, and TC* topologies that possess the opposite helicity of the PDLA microphase with similar chiral architectures were clearly observed.

Microphase transformation under thermodynamic condition

Chiral architectures constructed from the self-assembly of BCPs* have consistently been demonstrated to be kinetically dependent metastable structures rather than thermodynamically stable microphases.[31,32] In this study, colloidal particles containing chiral PDLA microphases

DOI: 10.31635/ccschem.021.202101067
CCS Chem. **2021**, *3*, 2561–2569

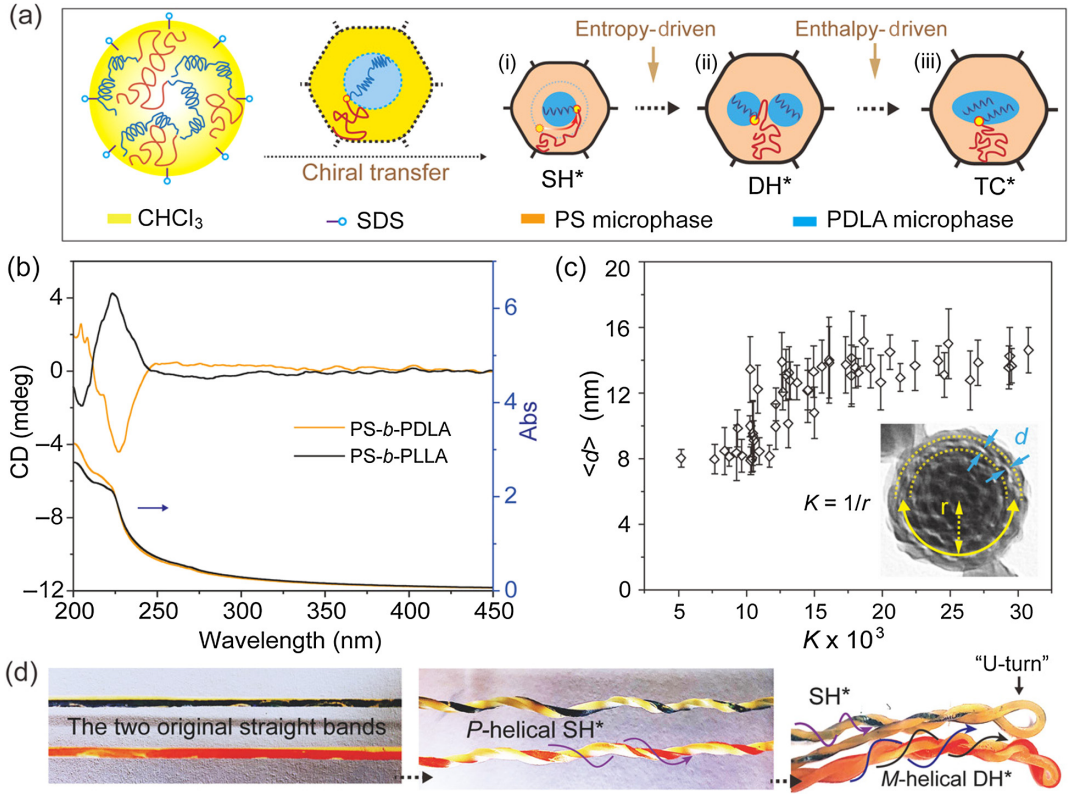

Figure 3 | *(a) Schematic description of conformation changes of PDLA and PS chains in the hexagonally packed microdomains during the hierarchical microphase transformations from premicrophase separation to SH*, to DH*, and to TC*. The PS and PDLA blocks with different conformations are illustrated by red and blue solid lines with different topologies, respectively. (b) The CD and UV–vis spectra of colloidal particles of PS-b-PDLA and PS-b-PLLA under the condition where the $C_{initial}$ is 10 mg/mL. (c) Counted results of the average section diameter (<d>) of PDLA cylinders along with curvature (K) in colloidal particles with different sizes. As shown in the inset, only the PDLA cylinders within the outer region of colloidal particles in TEM image were measured. (d) Photographs showing the spontaneos transformation of two adjacent rubber bands from SH* to DH*. Of note, the strain relaxation induced SH* to DH* transformation is completed for each rubber band rather than screwed together. "U-turn" forms at the end of DH* (Supporting Information Figure S14). SH* and DH* will coexist if the transformation from SH* to DH* is inadequate.*

were formed under fast solvent evaporation conditions, which preferentially induced metastable microphase structures due to the fast self-assembly kinetics of BCPs*. Solvent vapor annealing is a widely used method to efficiently enhance the chain mobility of BCPs and thus promote the microphase from a metastable state to a thermodynamically stable structure.[33,34] We utilized the solvent annealing method to further disclose the structural transformations of separated-microphase in the colloidal particle. Dramatic structural changes were observed in the internal microphases after annealing the preformed colloidal particles in $CHCl_3$ vapor (Figure 4a). TEM results clearly showed that the PDLA microphases displayed similar cylindrical microphases in colloidal particles with different sizes after solvent annealing (Figure 4b). 3D tomography TEM was utilized to further investigate the structures of these cylindrical microphases. Interestingly, we found that the PDLA microphase structures exhibited roughly mirror symmetry when rotated 90° along the normal axis, indicating that the PDLA cylinders displayed saddle-shaped topologies (Figure 4c and Supporting Information Video S3). The statistical <*d*> of PDLA cylinders in the colloidal particles further illustrated that the microphase structure of PDLA cylinders was size-independent (Figure 4d). The 1D SAXS profile for these colloidal particles exhibited reflections at the relative *q** values of $1:\sqrt{3}:\sqrt{4}:\sqrt{7}:\sqrt{9}$, suggesting a hexagonally packed cylindrical structure. Meanwhile, the increased lattice parameter (*a* = 32.0 nm) was very consistent with the statistical results of <*d*> (Supporting Information Figure S14). Therefore, an intriguing microphase transformation from chiral topologies including SH*, DH*, and TC* to achiral SC occurred during the solvent annealing.

The saddle-shaped topology probably preformed during the structural transformations from SH* to DH* and to TC* and further finalized upon solvent annealing

DOI: 10.31635/ccschem.021.202101067
CCS Chem. **2021**, *3*, 2561–2569

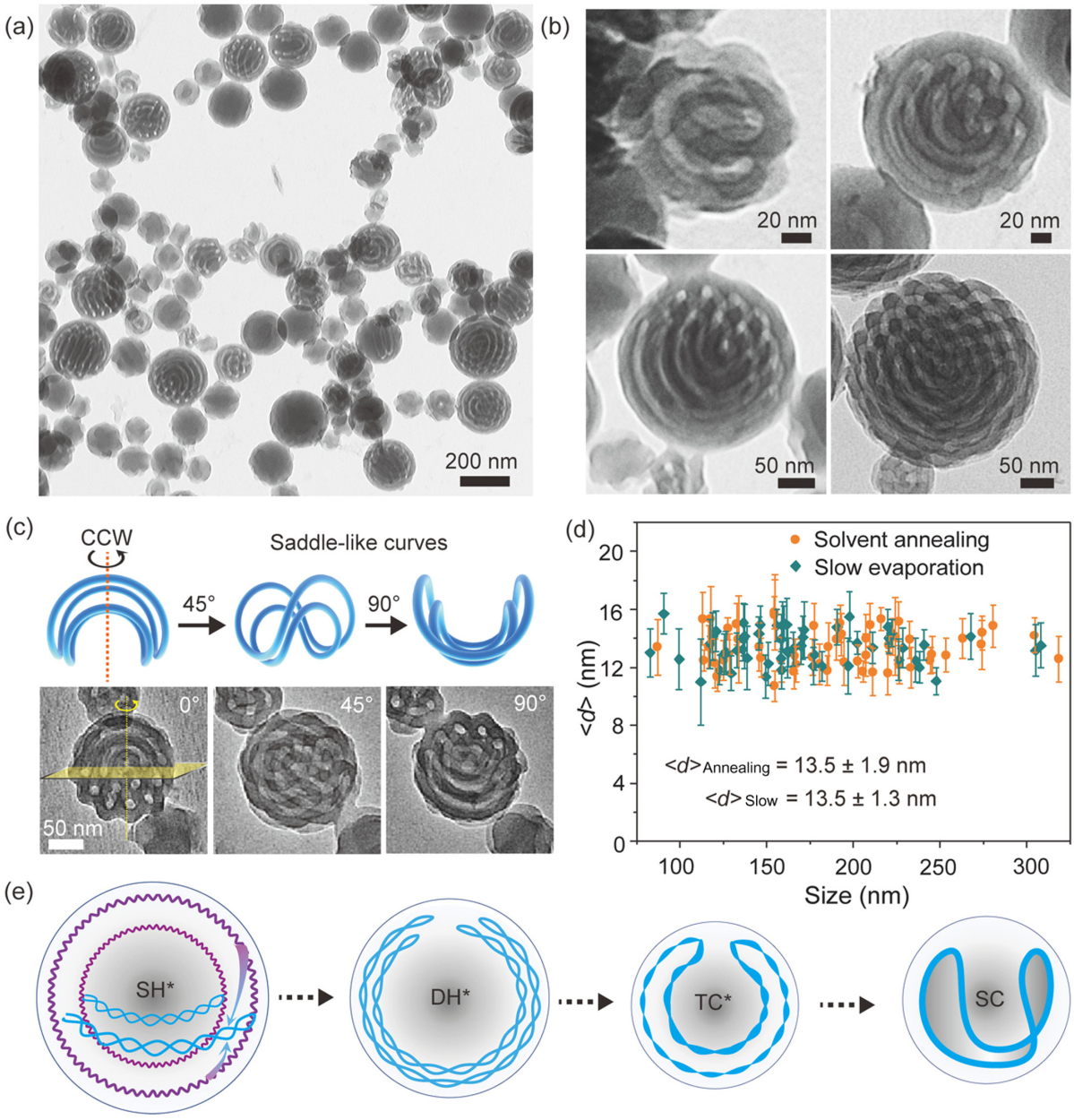

Figure 4 | *(a) TEM image of PS-b-PDLA colloidal particles after solvent annealing. The PDLA microphases were hydrolyzed by NaOH solution before characterization. (b) Magnified TEM images of representative mesoporous particles with different sizes. (c) Schematic illustration of the saddle-like curves viewed from different angles and corresponding 3D tomography TEM images of a representative colloidal particle under different view angles. Insets in TEM projective images show the horizontal plane, normal axis, rotation direction, and the corresponding rotation angles for each image. (d) Statistical results of <d> of SC in PS-b-PDLA colloidal particles obtained from solvent annealing of particles prepared from fast solvent evaporation and in PS-b-PDLA colloidal particles prepared from slow solvent evaporation. (e) Schematic illustration of the formation of saddle-like topology during the microphase transformations from SH* to DH*, to TC*, and to SC in a colloidal particle.*

(Figure 4e). During the relaxation of SH* into DH*, the two intertwined strands from SH* bent into an arc-like structure assisted by the spherical confined boundary. Upon further microphase transformation from DH* into TC*, the two screwed PDLA cylinders fused together, and the two adjacent endpoints (originated from "U-turns" (Supporting Information Figure S15)) docked together to minimize the PS/PDLA interfacial energy. The helical PDLA cylinders in colloidal particles underwent the above hierarchical structural transformations spontaneously

DOI: 10.31635/ccschem.021.202101067
CCS Chem. **2021**, *3*, 2561–2569

and synergistically, and as a consequence, directionally aligned SC formed. Moreover, the "self-avoiding" of PDLA cylinders in the colloidal particle was also assisted in the formation of saddle-like topology.[35] In short, the formation of the directionally aligned PDLA cylindrical microphase with SC topology was dominated by the synergistic effects between the hierarchical relaxation of the chiral effect and the self-avoiding of PDLA cylinders within the confined spherical geometry.

Pathway independence is a typical characteristic of the thermodynamic microphase structure.[36–38] We conducted a slow solvent evaporation control to further investigate the thermodynamic stable microphase structure within the colloidal particles from confined assembly of PS-*b*-PDLA. As expected, colloidal particles containing the same SC structure with a rather approximate <*d*> were constructed, compared to the colloidal particles obtained after solvent annealing (Figure 4d and Supporting Information Figure S16). This result further demonstrated that the SC is indeed a thermodynamic microphase structure for the confined assembly of PS-*b*-PDLA in emulsion droplets. Considering that the SC structure in colloidal particles is size-independent, it seems that the energy barriers for the structural transformations are substantially reduced upon solvent annealing. As a consequence, the proceeding of microphase transformations in big particles (D > 200 nm) is restarted, and eventually ends up as SC topology. This result verifies that the formation of those chiral architectures is kinetically dependent while their successive structural transformations are energetically favorable.

Conclusion

Successive structural transformations of chiral microphases from SH* to DH* to TC* and finally to achiral SC were demonstrated during the confined assembly of BCPs* in emulsion droplets. Both of the chiral segments and the achiral block of BCPs* are responsible for the above hierarchical microphase behaviors. Homochiral transfer of chiral segments from conformation to microphase determines the origination of chiral SH* topology, and the entropy loss of achiral blocks induces the microphase transformation from SH* to DH* with inverted helicity. Subsequently, the enthalpy effect promotes the microphase transformation from DH* to TC* and finally ends up as a thermodynamic achiral SC structure. The currently reported origination and subsequent structural transformation as well as the degeneration of chiral architectures are of fundamental significance for understanding chiral evolution at different length scales. Moreover, mesoporous particles containing sophisticated chiral nanochannels can be obtained after hydrolyzing the degradable chiral microphase, which is promising in polymer templates and in various particle-based applications.

Supporting Information

Supporting Information is available and includes additional information, tables, 1D SAXS profiles, X-ray photoelectron spectroscopy (XPS) spectra, CD spectra, TEM and scanning electron microscopy (SEM) images, schematic descriptions, and supporting videos.

Conflict of Interest

There is no conflict of interest to report.

Funding Information

This research was made possible as a result of a generous grant from the National Natural Science Foundation of China (nos. 51525302 and 21802049), the China Postdoctoral Science Foundation (no. 2017M622403) and the Innovation and Talent Recruitment Base of New Energy Chemistry and Devices (no. B21003).

Acknowledgments

Z.G. thanks Z. Chen for fruitful discussion. The authors thank Y. Zhou and X. Ren at Hubei University for SAXS measurements and the HUST Analytical and Testing Center and the School of Life Science and Technology for the use of their facilities.

References

1. Xing, P.; Zhao, Y. Controlling Supramolecular Chirality in Multicomponent Self-Assembled Systems. *Acc. Chem. Res.* **2018**, *51*, 2324–2334.
2. Lebreton, G.; Geminard, C.; Lapraz, F.; Pyrpassopoulos, S.; Cerezo, D.; Speder, P.; Ostap, E. M.; Noselli, S. Molecular to Organismal Chirality Is Induced by the Conserved Myosin 1D. *Science* **2018**, *362*, 949–952.
3. Zhang, Q.; Hernandez, T.; Smith, K. W.; Hosseini Jebeli, S. A.; Dai, A. X.; Warning, L.; Baiyasi, R.; McCarthy, L. A.; Guo, H.; Chen, D. H.; Dionne, J. A.; Landes, C. F.; Link, S. Unraveling the Origin of Chirality from Plasmonic Nanoparticle-Protein Complexes. *Science* **2019**, *365*, 1475–1478.
4. Liu, W.; Ji, Z.; Wang, Y.; Modi, G.; Hwang, M.; Zheng, B.; Sorger, V. J.; Pan, A.; Agarwal, R. Generation of Helical Topological Exciton-Polaritons. *Science* **2020**, *370*, 600–604.
5. Dou, X.; Mehwish, N.; Zhao, C.; Liu, J.; Xing, C.; Feng, C. Supramolecular Hydrogels with Tunable Chirality for Promising Biomedical Applications. *Acc. Chem. Res.* **2020**, *53*, 852–862.

6. Wang, P. P.; Yu, S. J.; Ouyang, M. Assembled Suprastructures of Inorganic Chiral Nanocrystals and Hierarchical Chirality. *J. Am. Chem. Soc.* **2017**, *139*, 6070–6073.
7. Ouyang, G.; Ji, L.; Jiang, Y.; Würthner, F.; Liu, M. Self-Assembled Moebius Strips with Controlled Helicity. *Nat. Commun.* **2020**, *11*, 5910.
8. Xu, P.; Gao, L.; Cai, C.; Lin, J.; Wang, L.; Tian, X. Helical Toroids Self-Assembled from a Binary System of Polypeptide Homopolymer and Its Block Copolymer. *Angew. Chem. Int. Ed.* **2020**, *59*, 14281–14285.
9. Wen, T.; Wang, H. F.; Li, M. C.; Ho, R. M. Homochiral Evolution in Self-Assembled Chiral Polymers and Block Copolymers. *Acc. Chem. Res.* **2017**, *50*, 1011–1021.
10. Lu, X.; Li, J.; Zhu, D.; Xu, M.; Li, W.; Lu, Q. Double-Helical Nanostructures with Controllable Handedness in Bulk Diblock Copolymers. *Angew. Chem. Int. Ed.* **2018**, *57*, 15148–15152.
11. Geng, Z.; Xiong, B.; Wang, L.; Wang, K.; Ren, M.; Zhang, L.; Zhu, J.; Yang, Z. Moebius Strips of Chiral Block Copolymers. *Nat. Commun.* **2019**, *10*, 4090.
12. Xu, L.; Wang, C.; Li, Y. X.; Xu, X. H.; Zhou, L.; Liu, N.; Wu, Z. Q. Crystallization-Driven Asymmetric Helical Assembly of Conjugated Block Copolymers and the Aggregation Induced White-light Emission and Circularly Polarized Luminescence. *Angew. Chem. Int. Ed.* **2020**, *59*, 16675–16682.
13. Cornelissen, J.; Fischer, M.; Sommerdijk, N.; Nolte, R. J. M. Helical Superstructures from Charged Poly(styrene)-Poly (isocyanodipeptide) Block Copolymers. *Science* **1998**, *280*, 1427–1430.
14. Wen, T.; Lee, J. Y.; Li, M. C.; Tsai, J. C.; Hoy, R. M. Competitive Interactions of π-π Junctions and Their Role on Microphase Separation of Chiral Block Copolymers. *Chem. Mater.* **2017**, *29*, 4493–4501.
15. Li, H.; Mao, X.; Wang, H. Y.; Geng, Z.; Xiong, B. J.; Zhang, L. B.; Liu, S. M.; Xu, J. P.; Zhu, J. T. Kinetically Dependent Self-Assembly of Chiral Block Copolymers under 3D Confinement. *Macromolecules* **2020**, *53*, 4214–4223.
16. Jones, J. J.; van der Maarel, J. R.; Doyle, P. S. Intrachain Dynamics of Large *ds*-DNA Confined to Slit-Like Channels. *Phys. Rev. Lett.* **2013**, *110*, 068101.
17. Japaridze, A.; Orlandini, E.; Smith, K. B.; Gmur, L.; Valle, F.; Micheletti, C.; Dietler, G. Spatial Confinement Induces Hairpins in Nicked Circular DNA. *Nucleic Acids Res.* **2017**, *45*, 4905–4914.
18. Pyne, A. L. B.; Noy, A.; Main, K. H. S.; Velasco-Berrelleza, V.; Piperakis, M. M.; Mitchenall, L. A.; Cugliandolo, F. M.; Beton, J. G.; Stevenson, C. E. M.; Hoogenboom, B. W.; Bates, A. D.; Maxwell, A.; Harris, S. A. Base-Pair Resolution Analysis of the Effect of Supercoiling on DNA Flexibility and Major Groove Recognition by Triplex-Forming Oligonucleotides. *Nat. Commun.* **2021**, *12*, 1053.
19. Wong, C. K.; Qiang, X. L.; Muller, A. H. E.; Groschel, A. H. Self-Assembly of Block Copolymers into Internally Ordered Microparticles. *Prog. Polym. Sci.* **2020**, *102*, 22.
20. Yang, Y.; Kang, T. H.; Wang, K.; Ren, M.; Chen, S. B.; Xiong, B. J.; Xu, J. P.; Zhang, L. B.; Yi, G. R.; Zhu, J. T. Tunable Photonic Microspheres of Comb-like Supramolecules. *Small* **2020**, *16*, e2001315.
21. Deng, R. H.; Xu, J. P.; Yi, G.-R.; Kim, J. W.; Zhu, J. T. Responsive Colloidal Polymer Particles with Ordered Mesostructures. *Adv. Funct. Mater.* **2021**, *31*, 2008169.
22. Deng, R. H.; Liang, F. X.; Li, W. K.; Liu, S. Q.; Liang, R. J.; Cai, M.; Yang, Z. Z.; Zhu, J. T. Shaping Functional Nano-Objects by 3D Confined Supramolecular Assembly. *Small* **2013**, *9*, 4099–4103.
23. Shin, J. J.; Kim, E. J.; Ku, K. H.; Lee, Y. J.; Hawker, C. J.; Kim, B. J. 100th Anniversary of Macromolecular Science Viewpoint: Block Copolymer Particles: Tuning Shape, Interfaces, and Morphology. *ACS Macro Lett.* **2020**, *9*, 306–317.
24. Lee, J. K.; Ku, H.; Kim, M.; Shin, J. M.; Han, J.; Park, C. H.; Yi, G.-R.; Jang, S. G.; Kim, B. J. Stimuli-Responsive, Shape-Transforming Nanostructured Particles. *Adv. Mater.* **2017**, *29*, 1700608.
25. Shin, J. M.; Kim, Y.; Yun, H.; Yi, G.-R.; Kim, B. J. Morphological Evolution of Block Copolymer Particles: Effect of Solvent Evaporation Rate on Particle Shape and Morphology. *ACS Nano* **2017**, *11*, 2133–2142.
26. Shin, J. M.; Kim, Y.; Ku, K. H.; Lee, Y. J.; Kim, E. J.; Yi, G.-R.; Kim, B. J. Aspect Ratio-Controlled Synthesis of Uniform Colloidal Block Copolymer Ellipsoids from Evaporative Emulsions. *Chem. Mater.* **2018**, *30*, 6277–6288.
27. Ho, R.-M.; Chiang, Y.-W.; Chen, C.-K.; Wang, H.-W.; Hasegawa, H.; Akasaka, S.; Thomas, E. L.; Burger, C.; Hsiao, B. S. Block Copolymers with a Twist. *J. Am. Chem. Soc.* **2009**, *131*, 18533–18542.
28. Ho, R.-M.; Li, M. C.; Lin, S.-C.; Wang, H.-F.; Lee, Y.-D.; Hasegawa, H.; Thomas, E. L. Transfer of Chirality from Molecule to Phase in Self-Assembled Chiral Block Copolymers. *J. Am. Chem. Soc.* **2012**, *134*, 10974–10986.
29. In, M.; Aguerre-Chariol, O.; Zana, R. Closed-Looped Micelles in Surfactant Tetramer Solutions. *J. Phys. Chem. B* **1999**, *103*, 7747–7750.
30. van der Gucht, J.; Besseling, N. A. M.; Fleer, G. J. Equilibrium Polymers at Interfaces: Analytical Self-Consistent-Field Theory. *Macromolecules* **2004**, *37*, 3026–3036.
31. Pashuck, E. T.; Stupp, S. I. Direct Observation of Morphological Tranformation from Twisted Ribbons into Helical Ribbons. *J. Am. Chem. Soc.* **2010**, *132*, 8819–8821.
32. Adamcik, J.; Mezzenga, R. Amyloid Polymorphism in the Protein Folding and Aggregation Energy Landscape. *Angew. Chem. Int. Ed.* **2018**, *57*, 8370–8382.
33. Vogelsang, J.; Brazard, J.; Adachi, T.; Bolinger, J. C.; Barbara, P. F. Watching the Annealing Process One Polymer Chain at a Time. *Angew. Chem. Int. Ed.* **2011**, *50*, 2257–2261.
34. She, M. S.; Lo, T. Y.; Ho, R. M. Controlled Ordering of Block Copolymer Gyroid Thin Films by Solvent Annealing. *Macromolecules* **2014**, *47*, 175–182.
35. Yu, B.; Li, B. H.; Jin, Q. H.; Ding, D. T.; Shi, A. C. Confined Self-Assembly of Cylinder-Forming Diblock Copolymers: Effects of Confining Geometries. *Soft Matter* **2011**, *7*, 10227–10240.
36. Han, Y.; Yu, H.; Du, H.; Jiang, W. Effect of Selective Solvent Addition Rate on the Pathways for Spontaneous Vesicle Formation of ABA Amphiphilic Triblock Copolymers. *J. Am. Chem. Soc.* **2010**, *132*, 1144–50.

DOI: 10.31635/ccschem.021.202101067
CCS Chem. **2021**, *3*, 2561–2569

37. Zhang, K.; Yeung, M. C.; Leung, S. Y.; Yam, V. W. Energy Landscape in Supramolecular Coassembly of Platinum (II) Complexes and Polymers: Morphological Diversity, Transformation, and Dilution Stability of Nanostructures. *J. Am. Chem. Soc.* **2018**, *140*, 9594–9605.

38. Adelizzi, B.; Aloi, A.; Markvoort, A. J.; Ten Eikelder, H. M. M.; Voets, I. K.; Palmans, A. R. A.; Meijer, E. W. Supramolecular Block Copolymers under Thermodynamic Control. *J. Am. Chem. Soc.* **2018**, *140*, 7168–7175.

DOI: 10.31635/ccschem.021.202101067
CCS Chem. **2021**, *3*, 2561–2569